COMPUTATIONAL ANALYSIS OF HYPERSONIC AIRBREATHING AIRCRAFT FLOW FIELDS

Douglas L. Dwoyer* and Ajay Kumar**
NASA Langley Research Center
Hampton, Virginia

Abstract

The general problem of calculating the flow fields associated with hypersonic airbreathing aircrafts is presented. Unique aspects of hypersonic airplane aerodynamics are introduced and their demands on CFD are outlined. Example calculations associated with inlet/forebody integration and hypersonic nozzle design are presented to illustrate the nature of the problems considered.

Introduction

Over the past several years, there has been a substantial increased interest in airbreathing propulsion systems for hypersonic airplanes. A hypersonic airplane powered by airbreathing engines can gain a performance advantage over a rocket powered vehicle by using the atmosphere as the oxidizer. In order to maintain this advantage, however, these airbreathing engines with their associated large capture areas must be closely integrated with the airframe aerodynamics in order to avoid excessive drag penalties. This requirement has led the Langley Research Center to pursue the development of the airframe integrated modular scramjet engine concept as shown in Figure 1. In this concept, the forebody is designed to provide the initial inlet compression through its bow shock, and the flared afterbody acts as a part of the nozzle. Cut-back cowls, spill windows, or spill doors must be provided on the inlets to allow startup over a wide Mach number range. Struts or centerbodies in the inlets may be necessary to provide additional compression and location for fuel injection.

Through the 1970's and early 1980's, research in hypersonic airbreathing propulsion focused on the development of the individual scramjet module. Since this research occured during the time period of rapid maturation of computational fluid dynamics (CFD), it was natural to develop CFD techniques for analyzing scramjet components. An excellent paper describing the development of CFD techniques for analyzing scramjet component flows is presented by White, et al.[1] According to Reference 1, inlet analysis techniques have reached a relatively high level of maturity, while techniques for combustor and nozzle analysis are somewhat less mature. For all of these components, however, Navier-Stokes (NS) and Parabolized Navier-Stokes (PNS) codes exist which account for all of the relevant physics. Further, as shown in Reference 1, the ability of the PNS and NS codes to account for three-dimensional viscous effects is crucial to the accurate prediction of component flows.

The same advancements in CFD technology that led to the scramjet engine component codes have also led to great improvements in the ability to predict hypersonic external aerodynamic flows. Throughout the 1970 interest in hypersonic, external aerodynamic predictions focused on reentry bodies and the shuttle orbiter. Sophisticated codes based on the viscous shock layer (VSL) approximation, as well as PNS and NS codes were developed for predicting hypersonic reentry body flows which included real gas, radiation, ablation, and wall catalysis effects. Codes such as the COLTS code[2] have been extensively validated and are widely used today for reentry bodies.

In dealing with complex, complete configurations such as the shuttle orbiter, a different strategy evolved for flow-field prediction. In this case, inviscid analysis codes based on solving the Euler equations were coupled with approximate three-dimensional viscous techniques to provide the required solution. The STEIN code,[3] a shock fit, space marching Euler code, was specifically developed for this purpose. STEIN was later followed by HALIS,[4] a time-dependent Euler code. In recent years, a complete vehicle viscous analysis capability for hypersonic aircraft has evolved around PNS and NS codes. The PNS/UNS approach[5] involves the use of both a PNS code and an unsteady Navier-Stokes (UNS) code to provide complete vehicle solutions about the shuttle orbiter. In Reference 6, an unsteady Navier-Stokes code has been used to provide the complete flow-field solution about the X-24C lifting body.

The flow-field analysis problem described above only deals with a part of the engineering problem of hypersonic aerodynamics. The analysis codes provide the engineer with flow-field data which

*Head, Computational Methods Branch, High-Speed Aerodynamics Division.

**Senior Research Scientist, Computational Methods Branch, High-Speed Aerodynamics Division.

can be used to derive aerodynamic performance information for given configurations. Another, and perhaps more important, problem is the development of the configurations themselves with some attempt at optimization subject to constraints. The use of analysis codes for the optimal design of hypersonic configuration components is a largely unexplored subject. A major exception is, of course, in the design of wind-tunnel and rocket nozzles where techniques based on the method of characteristics with boundary-layer correction have been in use for many years. These techniques are restricted to either two-dimensional or axisymmetric flows. Three-dimensional designs, or designs whose contraints force the relaxation of the requirement of shockless flow, will require more sophisticated CFD tools. The recent effort to design the aerolines for new nozzles for the NASA Langley Research Center 8' High Temperature Structures Tunnel[7] is an example of the kind of design project which can be undertaken using modern CFD techniques.

In summary, the status of CFD for analyzing the flow fields associated with hypersonic airbreathing airplanes is as follows. Full viscous analysis codes exist today for hypersonic gliders. Additionally, viscous analysis codes exist for the components of the most likely engine for hypersonic airplanes, the scramjet engine. Of these components, the inlet analysis capability is the most mature with somewhat less capable codes available for nozzles and combustors. Also, an attempt has been made to incorporate such codes into a design strategy for the nozzle portion of the flow field.

The time, thus, appears ripe to consider the extension of current CFD technology to one of the most crucial problems to be dealt with in the development of the hypersonic airbreathing airplane--propulsion/airframe integration. Additionally, further development of design strategies should occur over the next several years, with a heavy focus on inlets and nozzles. In this paper, we will first discuss the CFD requirements for hypersonic airplanes as compared to reentry vehicles. We will then review the status of the key CFD technologies incorporated into the current airframe and engine component codes. This will be followed by a discussion of the design problem using the constrained nozzle design problem as an example. Finally, we will discuss those areas of CFD technology requiring further development to deal with the propulsion/airframe integration problem.

CFD for Hypersonic Airplanes Vs. Reentry Vehicles

The hypersonic airplane concept places a somewhat different set of demands on CFD than does the reentry vehicle. Table I summarizes these differences in the view of the authors. The CFD demands for the hypersonic airplane stem largely from several dominating issues:

1. The requirement to fully integrate the airframe and propulsion system to achieve high Mach number performance.

2. The requirement that the vehicle be reusable with a minimum of refurbishment between flights.

3. The requirement to optimize vehicle performance over a wide Mach number range.

It is assumed herein that in both the airplane and reentry vehicle cases the flow fields have strong viscous effects. Thus, throughout the paper, emphasis will be on viscous flow-field prediction methods.

The development of a highly integrated airframe and propulsion system at high Mach numbers requires a CFD analysis capability which can treat flow fields of geometric complexity substantially greater than that of reentry vehicles including the Shuttle Orbiter. For example, an accurate prediction of the state of the three-dimensional boundary layer developed by the forebody at the inlet face is important for predicting installed inlet performance. The forebody geometry can be relatively simple, and the reusability of the vehicle implies a nonablative surface. Thus, the forebody flow-field analysis appears relatively straightforward in that the wall boundary conditions need not account for surface deformation and surface injection as would be the case with an ablative heat shield. On the other hand, an accurate prediction of this entire shock-layer profile is crucial in addition to the prediction of wall properties such as skin friction, heat transfer, and pressure. Such calculations are necessary to predict the shape of the bow shock and all embedded shocks as well as the mass and momentum flux entering the inlets. Of course, real gas effects on the forebody flow will become important for flight Mach numbers beyond about M = 10. Further, sophisticated surface boundary conditions which include wall catalysis effects and possible thermal deformation of the walls can be important in forebody flow-field prediction.

After the inlet face, the geometric complexity of the flow-field boundaries increases dramatically. At off-design

conditions, the inlets will spill a substantial amount of air thereby setting up a complex inlet/forebody flow-field interaction which can substantially effect both the inlet and forebody flow field. This flow region can be further complicated by the presence of wings. The geometric complexity of the forebody/multiple inlet/wing interacting flow field is far greater than the most geometrically complex reentry vehicles such as the Shuttle Orbiter.

The geometrical complexity of the forebody/inlet region extends to the aft end of the hypersonic airplane. The flow here is dominated by the interaction of the multiple internal/external nozzle system flow with the vehicle wing/body flow. The nozzle flow field will include real gas effects throughout the operating envelope of the vehicle, and at off-design conditions possible flow separation on the external nozzle surface must be accounted for. Requirements for accurate prediction of the complete three-dimensional flow field are again important on the external nozzle in order to estimate the nozzle thrust coefficient and the direction of the net thrust vector. Prediction of surface properties such as skin friction, heat transfer, and pressure are also vitally important. The real gas models incorporated in the nozzle flow analysis must include the chemistry of the combustor products as well as the air chemistry.

Engine combustor flow-field calculations require prediction of many complex physical phenomena not encountered on reentry vehicles. Important physical/chemical processes in the combustor include fuel/air mixing, ignition, combustion, and shock/turbulence interactions. The chemistry models in the codes must account for fuel combustion. There are a number of locations in a typical combustor where highly detailed analysis of very localized processes is required. Such regions include the immediate flow fields in the neighborhood of fuel injectors and flameholders. Accurate and detailed prediction of such highly localized phenomena is required if CFD is to be used in the analysis and design of combustors.

A major issue in CFD, common to both reentry vehicles and hypersonic airplanes, is transition and turbulence modeling. In transition modeling there is an important difference between the airplane and reentry vehicle, however. A typical reentry vehicle enters the atmosphere from above, and the flow transits from the rarefied state to the laminar continuum state to the turbulent continuum state. The hypersonic airplane, on the other hand, enters the atmosphere from below and goes from turbulent to laminar to rarefied. Transition and turbulence models for the hypersonic airplane must, therefore, account for this laminarization process. Important turbulence modeling issues for hypersonic airplane CFD are high Mach number mixing, shock/turbulent interaction, and three-dimensional separation. Real gas effects, very high Mach number compressibility effects, and kinetics/turbulence interaction are also important in the hypersonic airplane flow field.

The purpose of this discussion is not to argue that CFD for hypersonic airplanes is more difficult or complex than for reentry vehicles. Indeed, many crucial phenomena for the reentry vehicle such as transitional flow have been glossed over here. Rather, the thrust of this discussion is to point out that development of successful CFD analysis tools for hypersonic airplanes involves addressing a somewhat different set of problems. Given that hypersonic CFD has been primarily aimed at reentry problems for the past 25 years, it is clear that the hypersonic airplane CFD presents a variety of new research problems for the CFD community. Successful solutions of these problems will require an unprecedented level of cooperation between CFD researchers, experimentalists and theoreticians for many years to come.

Algorithms for Hypersonic Airplane CFD

The algorithms available today for computing the types of 3-D, viscous, hypersonic airplane flow fields described above can generally be categorized as: (1) parabolized Navier-Stokes (PNS) algorithms based on central-difference methods, (2) Reynolds averaged Navier-Stokes (RANS) algorithms based on central-difference methods, and (3) RANS algorithms based on upwind-difference methods. Of these three categories, PNS and RANS central-difference algorithms are the most mature and have been extended to include the most complete physical/chemical models. The upwind-difference based RANS codes are relatively new, and to date only perfect gas codes are available for the 3-D case. Thus, extensive research and code development work can be expected over the next several years to include more advanced physical and chemical models in upwind codes.

PNS Algorithms

The most widely used PNS codes today for high-speed viscous flow problems evolved from an implicit formulation first proposed by and later extended by Schiff and Steger.[8] This algorithm forms the basis of the AFWAL PNS code,[9] the NASA Ames PNS code,[5] and the PNS code of Gnoffo.[10] All of these codes rest on the assumption that there is a predominant flow direction which is roughly aligned

with one of the coordinate directions in a body fitted coordinate system. The steady RANS equations are then simplified by eliminating terms involving derivatives in the primary flow direction in the viscous stress tensor. Remaining derivatives, with repsect to the primary direction, are then upwind differenced and for flows whose Mach number components in the primary direction is entirely supersonic a well posed initial value problem ensues. The flow field may then be solved as a forward maching problem in the primary direction.

In order to make the discussion more concrete, it will be assumed that the PNS equations written on the x, y, z Cartesian coordinate system have been transformed to the curvilinear ξ,η,ζ coordinates. Here ξ is taken to be the primary flow, or marching, direction. In this case, the PNS equations become

$$\frac{\partial \hat{F}}{\partial \xi} + \frac{\partial(\hat{G} - \hat{G}_v)}{\partial \eta} + \frac{\partial(\hat{H} - \hat{H}_v)}{\partial \zeta} = 0 \qquad (1)$$

Here $\hat{F}$, $\hat{G}$, and $\hat{H}$ represent the inviscid part of the flux vectors and $\hat{G}_v$ and $\hat{H}_v$ represent the viscous part. Forming the discrete analog of Equation (1), the term $\partial F/\partial \xi$ will be replaced with an upwind difference while the $\partial/\partial\eta$ and $\partial/\partial\zeta$ terms will be replaced by central differences. In forming the discrete equations, one can choose either an explicit or implicit formulation in the marching direction. Gelda and McRae[11] have recently explored an explicit formulation of Equation (1) in 2-D, and this formulation holds promise of good efficiency on vector computers, particularly those which favor long vectors such as the CY-205. All of the 3-D codes are based on an implicit formulation, however. The implicit formulation takes the form

$$\frac{\frac{3}{2}\hat{F}^{i+1} - 2\hat{F}^{i} + \hat{F}^{i-1}}{\Delta\xi} + \bar{\delta}_\eta(\hat{G} - \hat{G}_v) + \bar{\delta}_\zeta(\hat{H} - \hat{H}_v)^{i+1} = 0 \qquad (2)$$

The superscript i denotes the grid point index in the ξ direction. Development of the solution algorithm for Equation (2) involves two steps; the first being linearization of the nonlinear terms, and the second an approximate solution of the linearized equations on the i+1 plane by approximate factorization. The linearization proceeds in a straightforward way from a Taylor expansion as

$$\hat{F}^{i+1} = \hat{F}^{i} + \left(\frac{\partial \hat{F}}{\partial U}\right)^{i}\Delta U + \ldots = \hat{F}^{i} + \hat{A}^{i}\Delta U$$

where

$$\Delta U = U^{i+1} - U^{i} \quad ;$$

U represents the conserved variables vector. With similar linearization in the η, ζ directions, the resulting equation assumes the form

$$\left[\frac{3}{2}\Delta\xi^{-1}\hat{A}^{i} + \bar{\delta}_\eta(\hat{B}^{i} - \hat{B}_v^{i}) + \bar{\delta}_\zeta(\hat{C}^{i} - \hat{C}^{i} - \hat{C}_v^{i})\right]\Delta U = -\left[\frac{-\frac{1}{2}\hat{F}^{i} + \hat{F}^{i-1}}{\Delta\xi} + \bar{\delta}_\eta(\hat{G} - \hat{G}_v)^{i} + \bar{\delta}_\zeta(\hat{H} - \hat{H}_v)^{i}\right] \qquad (3)$$

The system of Equation (3) with suitable additional artificial viscosity is then solved noniteratively on each successive i plane.

As discussed extensively by Chitsomboon, et al.[12], although Equation (3) is formally second-order accurate, the linearization of the ξ-difference term is not fully conservative. As shown in Reference 12, this lack of fully conservative differencing can lead to problems in accurate shock capturing. An example comparison between a PNS and RANS prediction of an inlet flow is shown in Figures 2 and 3. This calculation is for a 2-D scoop-type inlet. The calculations were done with the PNS code of Reference 5 and the RANS code of Reference 13. In Figure 2, the inlet geometry is shown along with plots of pressure versus axial distance through the inlet for both the scoop (top) surface and innerbody (bottom) surface. Examination of the scoop surface pressure shows a substantial difference in shock location and strength between the PNS and RANS prediction. Figure 3 shows the velocity vectors and pressure contours for the flow as predicted by the RANS calculation. The first pressure rise on the scoop is from the leading-edge shock, which reflects off the innerbody and hits the scoop at the second pressure rise. The PNS calculation predicts the formation of the leading-edge shock to be further downstream than the RANS calculation. The reflected shock intersection with the scoop is also more downstream in the PNS calculation as well as being substantially weaker. The shock reflection on the innerbody surface is also much weaker in the PNS case as well as far downstream. The RANS prediction indicates a small separation to be associated with the shock reflection from the innerbody, an effect not predicted in the PNS calculation. The scoop pressure comparison with data are far better for the RANS calculation than for the PNS calculation. The discrepancy between the calculations is attributed to the poor shock capturing of the PNS code along with too much artificial dissipation that allows it to march past the shock

reflection with no indication of separation. The PNS shock capturing error in this case, which is typical of a hypersonic inlet, leads to a completely erroneous flow-field prediction.

Central-Difference RANS Algorithms

CFD algorithms most commonly in use for high-speed RANS calculations are the MacCormack method[14] and the Beam and Warming method.[15] Both methods are designed to provide steady solutions to the RANS equations by embedding the steady problem in the properly posed time-dependent problem and marching the solution to large time with steady boundary conditions. For the hypersonic airplane problems, this approach has as its principle advantage over the PNS algorithms the ability to maintain fully conservative differencing. Additionally, this approach can accommodate separated flow in the streamwise direction.

The explicit methods have a substantial computer cost penalty associated with them when compared to the PNS approach or the implicit RANS approach. Unfortunately, the implicit RANS method of Beam and Warming suffers from stability restrictions in the 3-D case.[16] Thus, the explicit method is more robust than the implicit and it has been applied to a wider variety of problems associated with hypersonic airplanes as shown in References 1 and 5 and in the remainder of this paper. Additionally, inclusion of real gas effects is somewhat more straightforward in the explicit case than in the implicit case. Equilibrium gas chemistry has been incorporated into explicit algorithm codes by several authors including References 2, 7, and 17 and finite-rate chemistry in References 17 and 18.

A final point to be made about both types of central-difference RANS methods is about their shock capturing capability. Dissipative terms must be appended to the basic algorithms of References 14 and 15 to allow shock capturing. Very sophisticated artificial viscosity terms have been devised for this purpose which degrade the spatial accuracy of the methods only in the immediate vicinity of shocks. Even with the inclusion of these terms, the ability of central-difference codes to capture strong shocks is limited. Codes based on the central-differnce approach which are aimed at hypersonic flows generally rely on shock fitting to capture the bow shocks.

Upwind-Difference RANS Algorithms

In the last several years, an alternative to the central-difference approach has appeared which alleviates several of the difficulties mentioned with the central-differenced based PNS and RANS methods. This alternative has its basis in the total variation dimishing (TVD) methods developed by solving the Euler equations in the early 1980's. A number of investigators have combined these TVD methods for the convective terms in the RANS equations with central differencing to the viscous terms to yield this new class of algorithms. Methods under current development include those of References 19, 20, 21, and 22. This new class of algorithms is herein refered to as the upwind RANS algorithm.

The upwind RANS methods generally retain the superior shock capturing capability of the Euler method on which they are based. The method can be implemented in both explicit and implicit form, with the majority of implementation to date being implicit. In the implicit form, the coefficient matrix associated with the change in the dependent variable vector is in relatively well conditioned and hence a number of innovative new solution strategies have evolved for the upwind methods. In addition to the conventional three factor ADI approach for solving the implicit upwind RANS equation,[23] relaxation methods have also been introduced. The use of planar Gauss-Seidel relaxation has been used by a number of authors. Walters and Dwoyer[24] have also shown that this technique can serve as the basis for an algorithm for combining the PNS and RANS approach.

The upwind RANS methods have not been extended to include real gas effects to date. There is no fundamental restriction on such an extension, and a number of groups are currently exploring real gas upwind RANS methods. Until these extensions are proven, applicability of the upwind RANS methods to the hypersonic airplane problem will be limited.

Algorithm Summary

The comments presented above can be summarized in the following way. The central-difference PNS algorithms are the least expensive of the currently available methods for computing hypersonic airplane flow fields. They are useful for problems in which the shocks radiate out of the computational domain without interacting with vehicle components. For situations where the shocks can impinge on vehicle components, or for the internal flow case, the central-difference PNS methods are generally unsatisfactory due to their nonconservative property.

The central-difference RANS methods are today the most general and useful methods. The most popular explicit and implicit solution algorithms have shortcomings in computational complexity and stability respectively which has led to the search for alternatives. Additionally, the central-difference

methods are limited in shock capturing capability. Despite this, as will be demonstrated later in the paper, they are currently the algorithms of choice for complex hypersonic airplane flow-field prediction.

The upwind RANS methods alleviate several of the central-difference method shortcomings. The solution algorithms appear to be more robust and they possess superior shock-capturing capability. To date, however, the applicability of the method to the hypersonic airplane problem is still in the exploratory stage.

Real Gas Effects

The high temperatures encountered in hypersonic flight can lead to vibrational excitation, dissociation, and ionization of the air. These high temperatures would occur in the blunted regions of the vehicle due to strong shocks and in the boundary layers due to extreme viscous dissipation. Further complicating factors that may need to be considered are radiative heating and deformation of the surface, and surface catalysis for chemical reactions. Additionally, in the analysis of combustor and nozzle flows, the fuel/air chemistry must be considered. These high-temperature reacting flows can have significant influence on the vehicle and propulsion system performance. Generally speaking, at moderate hypersonic Mach numbers, the reaction rates associated with the air chemistry are fast enough that the air may be considered in chemical equilibrium but at higher hypersonic Mach numbers, the effects of nonequilibrium chemistry must be considered.

Inclusion of nonequilibrium chemistry in the codes results in significant complexity and increased computational time whereas equilibrium chemistry can be added rather easily. Most advanced flow-field analysis codes still do not have nonequilibrium chemistry whereas equilibrium chemistry is being added to a significant number of codes. A brief description is given below on how the equilibrium gas chemistry can be included in the code.

In the equilibrium gas chemistry approach, the gas is assumed to be in chemical and thermodynamic equilibrium at all points in the flow field. The simplest way to include these effects is through the use of variable equivalent gamma (VEG) approach.[2,10] Gamma is determined by assuming a locally linear relationship between temperature and enthalpy at every grid point. The enthalpy, in turn, is calculated from a benchmark equilibrium code such as EQUIL.[25] The code EQUIL uses free energy minimization technique to calculate mixture composition, its enthalpy and molecular weight and other thermodynamic and transport properties given the pressure, temperature, and elemental composition of the mixture as input. This code is very general and can be used in situations with surface mass addition, ablation, etc. For simple air chemistry only, one can use other simpler equilibrium chemistry routines. The preceding VEG approach can be included in any perfect gas code with relatively little effort.

The real gas effects start to show up for freestream Mach numbers greater than ten in atmospheric flight. Figure 4 shows typical velocity, temperature, and pressure profiles in a cone shock layer at two flight Mach conditions in air, the first at $M = 10$ and the second at $M = 24.5$. The most important effect of gas property variation is on the temperature profile, and hence also on the heat transfer.

Advanced Applications

This section presents examples of some advanced applications of CFD in analysis and design studies. In the first application, integration and interaction of multiple inlet modules are studied whereas in the second application, the use of CFD codes is demonstrated in nozzle design subject to some external constraints.

Multiple Module Inlet Integration

As mentioned in the preceeding sections, one of the major requirements in the development of the hypersonic vehicle is to closely integrate the vehicle airframe and the propulsion system. In an effort to investigate this problem, an experimental as well as analytical program has been devised at NASA Langley. The goal of this program is to predict performance and interactins of multiple scramjet inlets mounted on the vehicle undersurface. Figure 5 shows the schematic of the test model. It has three modules mounted on a flat plate that simulates the forebody boundary layer. The compression sufaces of each module are swept wedges. The aft body expansion is simulated by an expansion on the plate. Experimentally, the model will be tested over a Mach number range, small angles of attack, and possibly some yaw. The experimental results will be compared against the numerical result obtained from a three-dimensional Navier-Stokes code.[26] This code solves the governing equations in conservation form by MacCormack's method. It has an algebraic eddy viscosity model for turbulent flow and is highly vectorized for VPS 32 (an upgraded CDC CYBER-200 series computer) or CRAY computers. No experimental results are

yet available, but a series of numerical calculations have been made using the expected geometry of the test model and tunnel flow conditions. Sample results from one such calculations are presented here. The flow conditions used in the calculation are as follows:

$M_\infty = 4.03$

$p_\infty = 8724\ N/m^2$

$T_\infty = 70K$

Each inlet module has a geometric contraction ratio of 4.0, and the cowl closure begins at the throat of the inlets. The results presented here are for zero angle of attack and yaw.

Figure 6 shows the grid in a cross plane and the symmetry plane of the configuration beginning from the face of the inlet modules. The extended portion of the grid below the cowl in the symmetry plane is for accounting the interaction between the internal and external fow. This interaction arises due to the aft placement of the cowl that exposes the high-pressure internal flow to the low-pressure external flow. The grid in the cross plane shows grid lines going through the module sidewalls. This is done to avoid elaborate grid generation procedure which will be required to embedd the module sidewalls which are not present in the extended region of the grid under the cowl. If a cross plane lies above the cowl plane, the grid points lying within the sidewalls are ignored and suitable boundary conditions are applied on the surface of the sidewalls but if the cross plane lies below the cowl plane, all the grid points are used in the analysis. The calculations presented here are made with a grid of about 340,000 points (61 points in the x-direction, 91 points in the y-direction, and 61 points in the z-direction). Only half of the configuration is analyzed due to flow symmetry at zero angle of attack and yaw. Out of the 61 grid planes in the z-direction, 25 planes lie below the cowl plane to account for the end effects.

A two-dimensional Navier-Stokes code[13] is used on the front part of the flat plate to calculate the profiles of flow quantities as the flow approaches the modules. The three-dimensional code is then used for the flow from the face of the modules to the end of the configuration. Figure 7 shows the velocity vector field and pressure contours in a cross plane located slightly above the cowl plate. Slight blunting of the sidewall leading and trailing edges, caused by the grid lines through the sidewalls, is obvious. Pressure contours show the shock and expansion waves and their interactions. Since it is a cold flow with no fuel injection, the flow expands back to low pressure behind the inlet throat. The velocity vector plot shows relatively small regions of separated flow caused by the shock/boundary-layer interactions.

Figure 8 shows the pressure contours and velocity vector field in the plane of symmetry. The velocity vector plot shows a significant downturn in flow direction ahead of the cowl resulting in some flow spillage. The downturn is caused by the sidewall sweep and the interaction between the internal and external flow. Once the inlet flow passes behind the cowl leading edge, it is turned back parallel to the cowl plane, and this turning result in a cowl shock which is evident in the pressure contour plot. Other features of flow are maked on the figure.

As mentioned earlier, not all the flow approaching the inlet modules is captured by them. Some of it is spilled out due to the swept compression surfaces and effects. Figure 9 shows axial distribution of the capture. It is seen that a significant amount of flow is spilled ahead of the cowl.

Although not included here, calcuations have also been made at small angles of attack and yaw. These results will be compared with the experimental results when available.

Multiple Inlet Interactions

One of the concerns that need to be investigated both numerically as well as experimentally is the potential for interactions between closely mounted multiple inlets. In order to examine the potential for such interactions, a two-strut scramjet inlet shown in Figure 10 is used as a model problem for a three-inlet system. As is seen, the inlet has three separate passages. The two center struts have an initial compression angle of 9°, and the initial cowl closure begins at the throat for which $x/x_T = 1$. To study the interactions, an attempt is made to unstart the center passage and see the impact of this unstart on the two side passages. In the initial attempts to unstart the center passage, the cowl location is fixed at the throat but the geometric contraction ratio of the center passage, W/G, is increased substantially by increasing the strut compression angle from 9° to 10.75°. This increase in center passage contraction ratio did not cause it to choke and resulted in no interaction with the side passages as is evident from the pressure contours in Figure 11 which remain unchanged with increase contraction ratio. However, the increased contraction ratio results in much higher pressure in the center passage as well as a increased downturn of the

flow ahead of the cowl as is seen from Figures 12 and 13. A capture plot of the inlet is shown in Figure 14. It is seen that as the center passage is gradually closed, the total inlet capture goes down, but the capture plots of individual passages show that all the decrease in capture is due to the increased spillage from the center passage. The capture of the side passages remains constant. This again confirms that there is no interaction between the center and side passages.

The second attempt to choke the center passage is made by moving the cowl forward from its initial location of $x/x_T = 1$. Two cowl locations of $x/x_T = .85$ and $.67$ are tried with strut compression angle remaining at 9°. For both cowl locations, the center passage still did not choke but the inlet capture increased significantly as is seen from Figure 15. But for $x/x_T = .67$, when the strut compression angle is increased to 10°, choking or unstart of the center passage is observed. Figure 16 shows the pressure contours in the symmetry plane of the inlet. The results of 9° strut compression angle are used as the starting solution. Pressure contours at 5,500, 10,000, 13,000, and 17,500 clearly show the development and formation of a bow shock ahead of the cowl. This bow shock stands in front of the cowl producing a region of subsonic flow between the shock and the cowl and resulting in significantly increased spillage from the center passage. The pressure contours in the cross plane located slightly above the cowl plane are shown in Figure 17. It is seen that the flow in the side passages has also been modified due to the unstart of the center passage. Obviously, once the subsonic flow ahead of the cowl is established, it interacts with the flow in the side passages and modifies it.

Nozzle Design

The analysis codes are still not widely used in the design of hypersonic configuration components. A major exception is, of course, in the design of wind tunnel and rocket nozzles where techniques based on method of characteristics with boundary-layer correction have been in use for many years. These design techniques are restricted to either two-dimensional or axisymmetric flows. Three-dimensional designs or designs whose constraints force the relaxation of the requirement of shockless flow, will require more sophisticated CFD tools. The recent effort to design the nozzle contours for the NASA Langley 8' High-Temperature Tunnel (HTT) provides an example of the use of advanced CFD codes in design projects. Under this effort, two nozzles for Mach 4 and 5 are being designed such that they smoothly blend with the existing Mach 7 nozzle about 200 inches upstream of the test section. The specified contraints are: (1) the axial position and radius of the entrance to the subsonic region; (2) the throat axial location; and (3) the axial station where current and new nozzle walls must smoothly blend together. The Mach number variaton is required to remain below ±0.1 about its mean value across 60% of the core flow. The high temperature flow in the tunnel requires the possibility of foreign gas injection for transpiration cooling in the nozzle throats. Furthermore, the large static temperature variation in the nozzles leads to a significant variation in gas properties, and those variations must be properly modeled.

Due to the imposed constraints, it was found that the conventional shockless nozzle design procedure was not applicable. A new iterative design procedure was developed in the present effort that couples an Euler code, a method of characteristics code, and boundary-layer code. A Navier-Stokes code is used to check the overall flow quality of the final design. All codes include consistent real gas chemistry packages for H-C-O-N gas system. In addition, the Navier-Stokes and boundary-layer codes have the capability to account for foreign gas injection for transpiration cooling. A detailed discussion of this iterative design procedure is given in Reference 7.

Figures 18 and 19 show some results obtained from the design of the Mach 5 nozzle. Figure 18 shows the Mach number profiles in the exit plane of the nozzle calculated by the Navier-Stokes and Euler codes. The profile has a mean value of 4.96 with a variation of ±0.06 over more than 70% of the test section radius, thus satisfying the Mach number variation constraint. However, a weak shock forms near the nozzle throat and intersects the exit plane, as is clearly seen from the Mach number contours in Figure 19. It appears that the weak shock cannot be avoided under the present geometric constraints. Figures 18 and 19 also illustrate the qualitative similarities in the flow solution obtained from the iterative design procedure and the Navier-Stokes code.

The preceeding design procedure is general and can easily be modified to treat perfect gas or any other real gas mixture.

Conclusions

The purpose of this paper has been to discuss CFD technology as it relates to the computation of flow fields associated with hypersonic airbreathing airplanes. It has been shown that the unique aerodynamics of these vehicles places

different demands on CFD than reentry body aerodynamics does. The major areas requiring the use of advanced CFD techniques are the prediction of airframe aerodynamics, propulsion/airframe flow-field interaction, and internal engine flows. All of these applications require use of 3-D viscous codes, most often RANS codes. PNS codes appear to have limited applicability to the hypersonic airplane problem. Advances in algorithm robustness and speed, geometric flexibility, and inclusion of real gas effects are required in the 3-D Navier-Stokes codes if they are to be widely used in the development of hypersonic airbreathing airplanes.

References

1. White, M. E.; Drummond, J. P.; and Kumar, A.: Evolution and Status of CFD Techniques for Scramjet Applications. AIAA Paper No. 86-0160, Jan. 1986.

2. Kumar, A.; Graves, R. A., Jr.; Weilmuenster, K. J.; and Tiwari, S. N.: Laminar and Turbulent Flow Solutions with Radiation and Ablation Injection for Jovian Entry. AIAA Paper No. 80--0288, Jan. 1980.

3. Marconi, F.; and Yaeger, L.: Development of a Computer Code for Calculating the Steady Super/Hypersonic Inviscid Flow Around Real Configurations. NASA CR-2676, May 1976.

4. Weilmeunster, K. J.; and Hamilton, H. H., II: Calculation of Inviscid Flow Over Shuttle-Like Vehicles at High Angles of Attack and Comparisons With Experimental Data. NASA TP-2103, May 1983.

5. Chaussee, D. S.; Rizk, Y. M.; and Bunning, P. G.: Viscous Computations of a Space Shuttle Flow Field. NASA TM-85977, June 1984.

6. Shang, J. S.; and Scherr, S. J.: Navier-Stokes Solution of the Flow Field Around a Complete Aircraft. AIAA Paper No. 85-1509 CP, July 1985.

7. Erlebacher, G.; Kumar, A.; Anderson, E. C.; Rogers, R. C.; Dwoyer, D. L.; Salas, M. D.; and Harris, J. E.: A Computational Design Procedure for Actively Cooled Hypersonic Wind-Tunnel Nozzles Subject to Wall Shape Constraints. Proceedings of Computational Fluid Dynamics in Aerospace Design Workshop, University of Tennessee Space Institute, UTSI Pub. EO2-4005-029-85, June 1985.

8. Schiff, L. B.; and Steger, J. L.: Numerical Simulation of Steady Supersonic Viscous Flow. AIAA Paper No. 79-0130, Jan. 1979.

9. Kaul, U. K.; and Chaussee, D. S.: AFWAL Parabolized Navier-Stokes Code: 1983 AFWAL/NASA Merged Baseline Version. AFWAL-TR-83-3118, May 1984.

10. Gnoffo, P. A.: Hypersonic Flows Over Biconics Using a Variable-Effective Gamma, Parabolized Navier-Stokes Code. AIAA Paper No. 83-1666, July 1983.

11. Gielda, T.; and McRae, D.: An Accurate, Stable, Explicit, Parabolized Navier-Stokes Solver for High-Speed Flows. AIAA Paper No. 86-1116, May 1986.

12. Chitsomboon, T.; Kumar, A.; and Tiwari, S. N.: A Parabolized Navier-Stokes Algorithm for Separated Supersonic Internal Flows. AIAA Paper 85-1411, July 1985.

13. Kumar, A.: Numerical Analysis of the Scramjet Inlet Flow Field by Using Two-Dimensional Navier-Stokes Equations. NASA TP-1940, Dec. 1981.

14. MacCormack, R. W.: The Effect of Viscosity in Hypervelocity Impact Cratering. AIAA Paper No. 69-354, 1969.

15. Beam, R.; and Warming, R. F.: An Implicit Factored Scheme for the Compressible Navier-Stokes Equations. AIAA Journal, vol. 16, April 1978, pp. 393-402.

16. Abarbanel, S.; Dwoyer, D. L.; and Gottlieb, D.: Stable Implicit Finite-Difference Methods for Three-Dimensional Hyperbolic Systems. ICASE Report No. 82-39, 1982.

17. Gnoffo, P. A.; and McCandless, R. S.: Three-Dimensional AOTV Flow Fields in Chemical Nonequilibrium. AIAA Paper No. 86-0230, Jan. 1986.

18. Uenishi, K.; Rogers, R. C.; and Northam, G. B.: Three-Dimensional Computations of Transverse Hydrogen Jet Combustion in a Supersonic Airstream. AIAA Paper No. 87-0089, Jan. 1987.

19. Thomas, J. L.; and Walters, R. W.: Upwind Relaxation Algorithms for the Navier-Stokes Equations. AIAA Paper No. 85-1501 CP, July 1985.

20. Gnoffo, P. A.; McCandless, R. S.; and Yee, H. C.: Enhancements to Program LAURA for Computation of 3-D Hypersonic Flow. AIAA Paper No. 87-0280, Jan. 1987.

21. Chakravarthy, S. R.; Szema, K-Y.; Goldberg, U. C.; and Gorski, J. J.: Application of a New Class of High

Accuracy TVD Schemes to the Navier-Stokes Equations. AIAA Paper No. 85-0165, Jan. 1985.

22. Lombard, C. K.; Bardina, J.; Venkatapathy, E.; Yang, J. Y.; Luh, R. C-C.; Nagaraj, N.; and Raiszadeh, F.: Accurate, Efficient, and Productive Methodology for Solving Turbulent Viscous Flows in Complex Geometry. Tenth Intl. Conf. on Numerical Methods in Fluid Dynamics, June 1986.

23. Anderson, W. K.; and Thomas, J. L.: Multigrid Acceleration of the Flux Split Euler Equations. AIAA Paper No. 86-0274, Jan. 1986.

24. Walters, R. W.; and Dwoyer, D. L.: An Efficient Iteration Strategy Based on Upwind/Relaxation Schemes for the Euler Equations. AIAA Paper No. 85-1529-CP, July 1985.

25. Kumar, A.; Graves, R. A., Jr.; and Weilmeunster, K. J.: Users Guide for Vectorized Code EQUIL for Calculating Equilibrium Chemistry on Control Data Star-100 computer. NASA TM-80193, April 1980.

26. Kumar, A.: Numerical Simulation of Scramjet Inlet Flow Fields. NASA TP-2517, May 1986.

TABLE I

REENTRY BODY VS. HYPERSONIC AIRPLANE CFD

REENTRY	HYPERSONIC AIRPLANE
Axisymmetric and 3-D	3-D
Simple Wave System	Complex Wave System
	Shock/Boundary-Layer Interactions
Wall Effects - Ablation/Injection - Catalysis - Roughness/Deformation	Wall Effects - Catalysis - Thermal Deformation - Local Injection
Gas Model - Transition/Turbulence - Air Chemistry - Radiation	Gas Model - Transition/Turbulence - Laminarization - Air & Fuel Chemistry
Simple Geometry	Complex Geometry
External	External/Internal
Projectile/Glider	Powered
	Design/Optimization

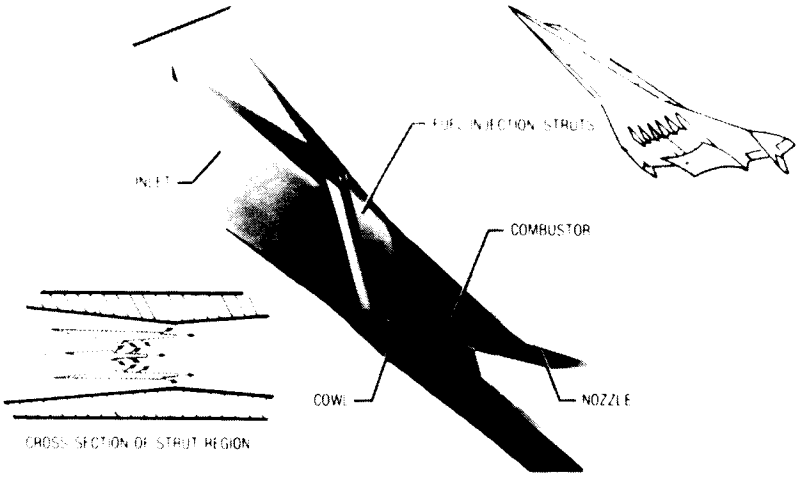

Fig. 1.- Scramjet engine module and its cross section.

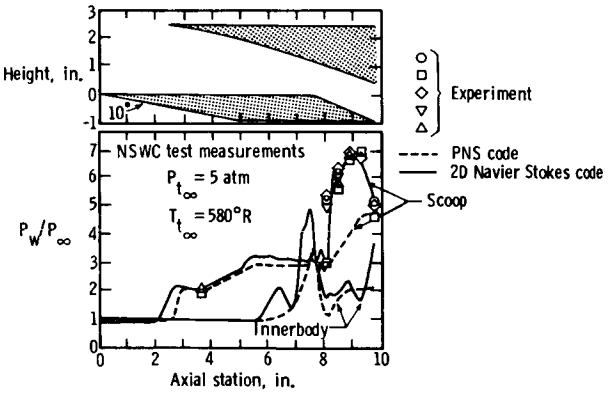

Fig. 2.- Surface pressure distribution for the 2-D multiple inward-turning scoop inlet model.

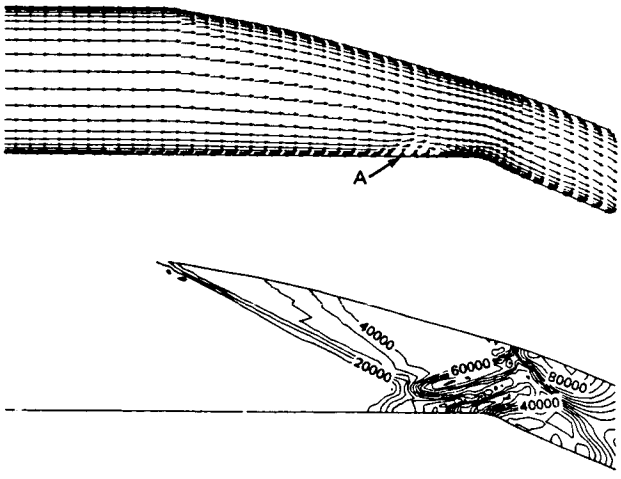

Fig. 3.- Velocity vector field and pressure contours for the 2-D multiple inward-turning scoop inlet model.

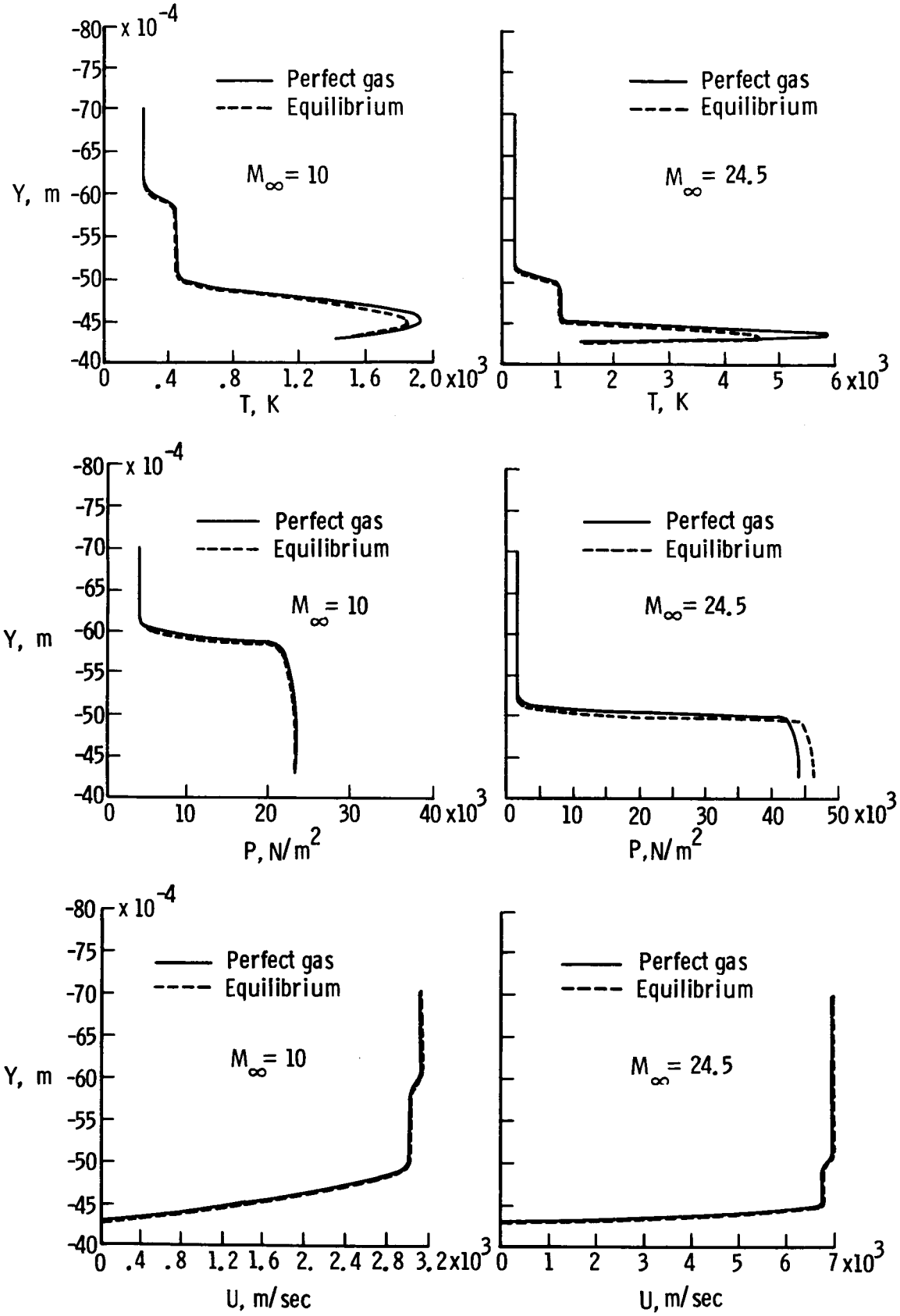

Fig. 4.- Perfect and equilibrium gas shock-layer profiles over a cone.

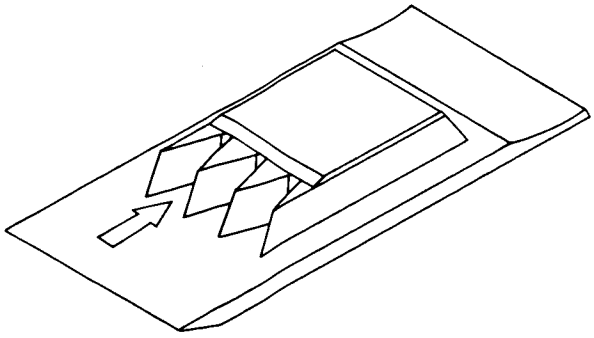

Fig. 5.- Schematic of a multiple module scramjet engine.

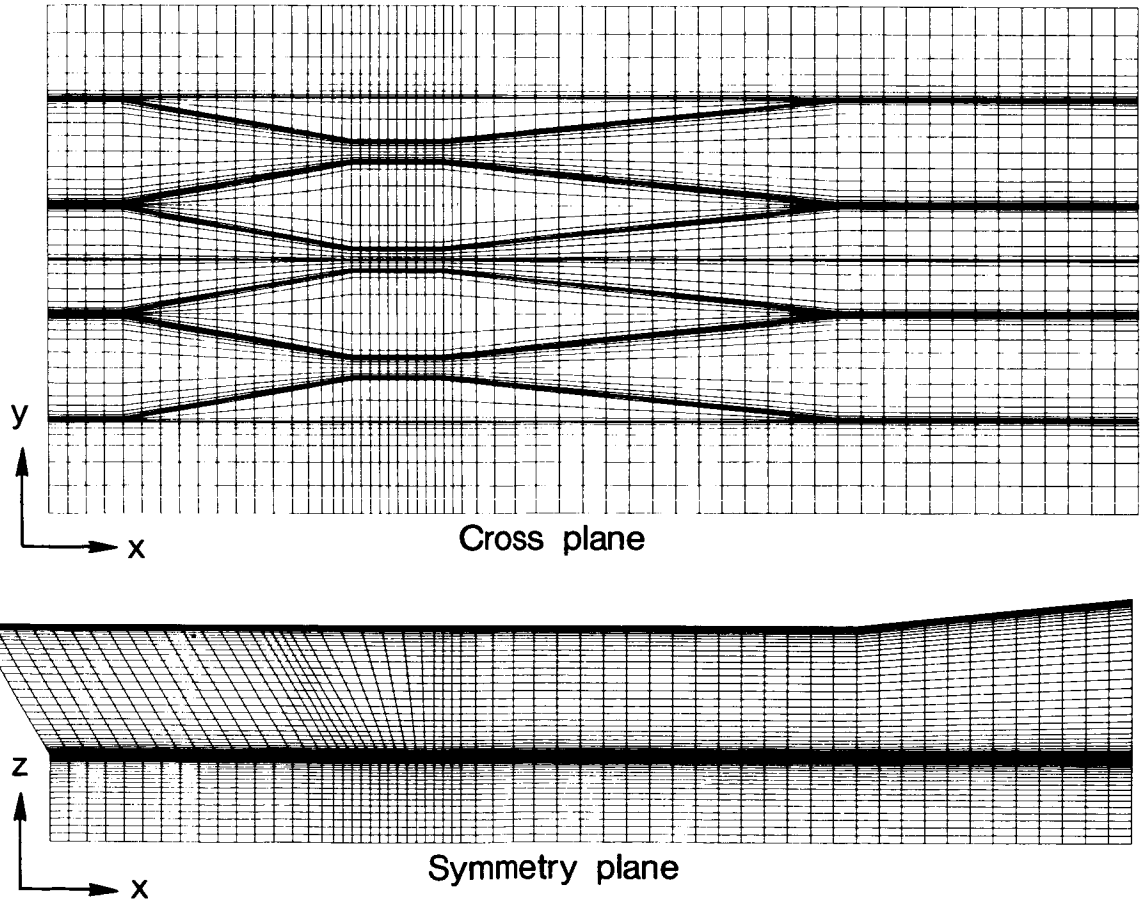

Fig. 6.- Computational grid.

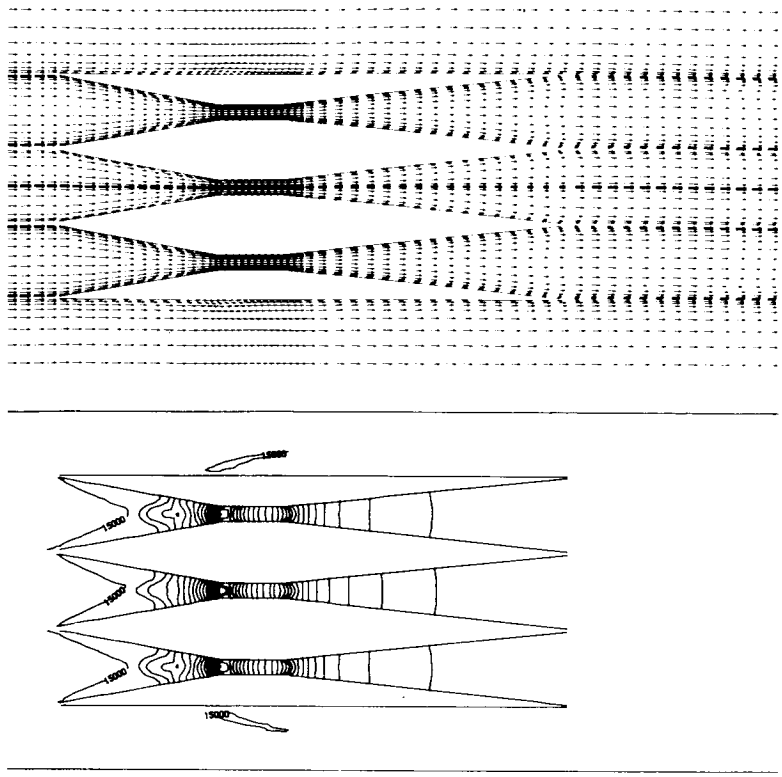

Fig. 7.- Velocity vector field and pressure contours in a cross plane slightly above the cowl plane.

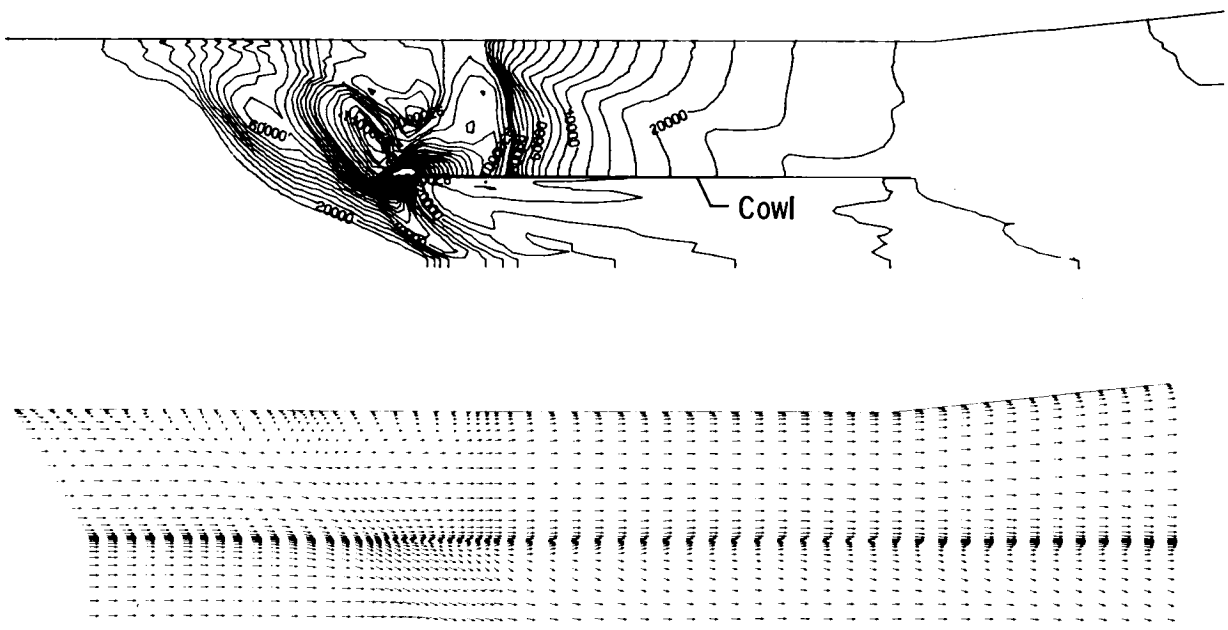

Fig. 8.- Pressure contours and velocity vector field in the symmetry plane.

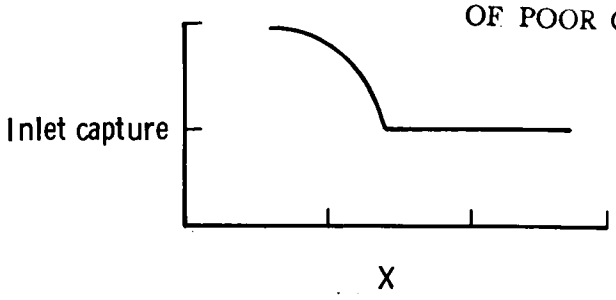

Fig. 9.- Axial capture distribution.

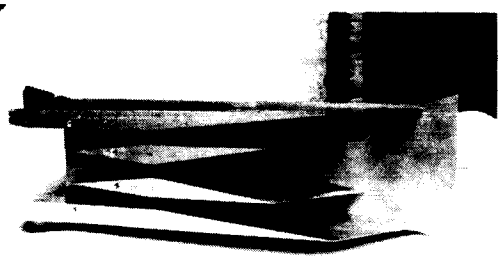

Fig. 10.- Two-strut scramjet inlet.

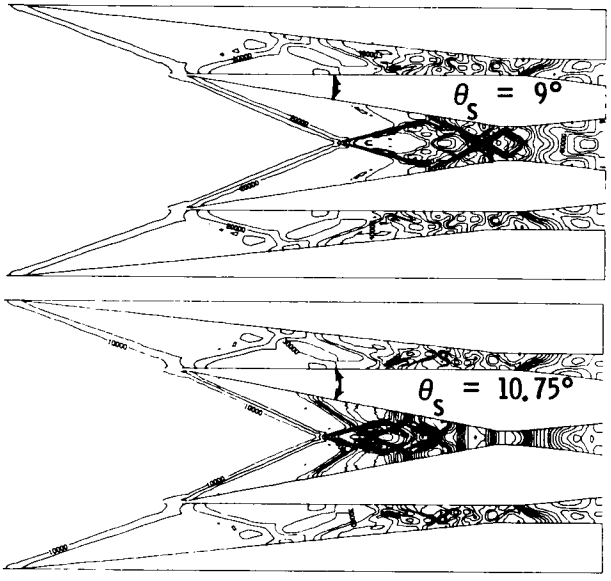

Fig. 11.- Pressure contours in a cross plane located at 12% of the inlet height from the cowl plane.

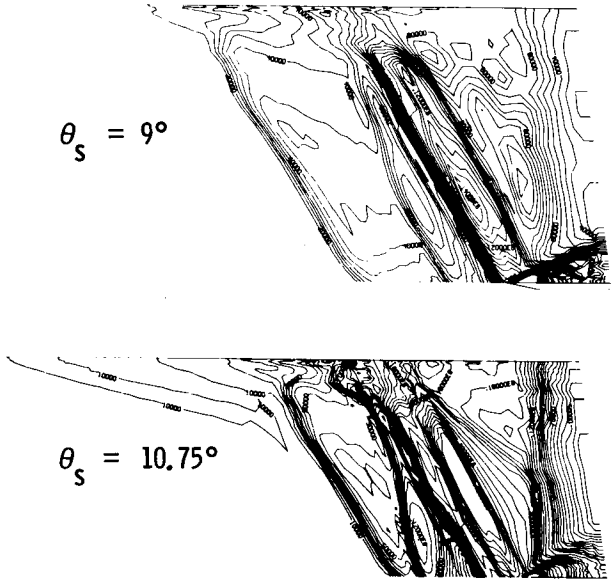

Fig. 12.- Pressure contours in the symmetry plane.

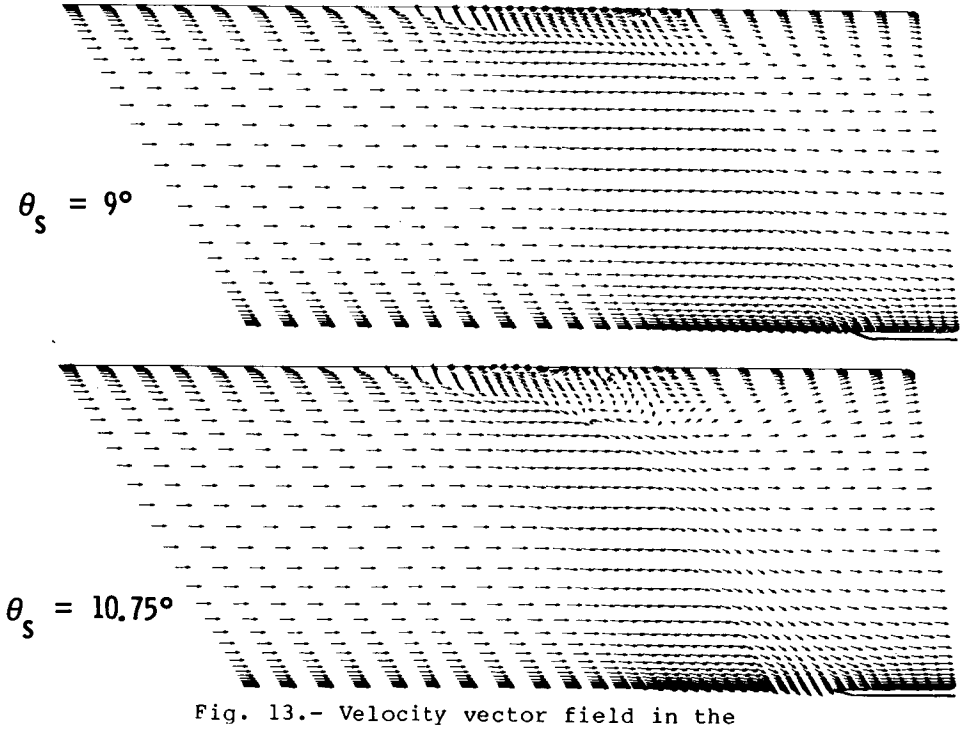

Fig. 13.- Velocity vector field in the symmetry plane.

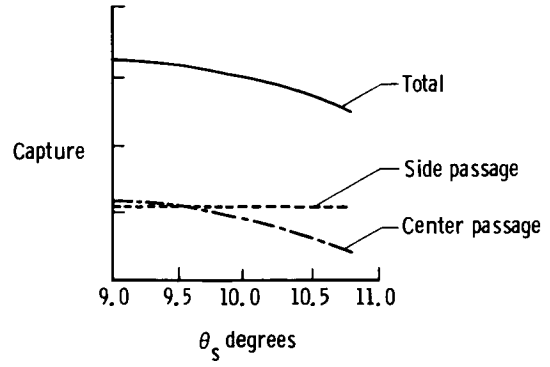

Fig. 14.- Inlet capture as a function of strut compression angle, θ_s.

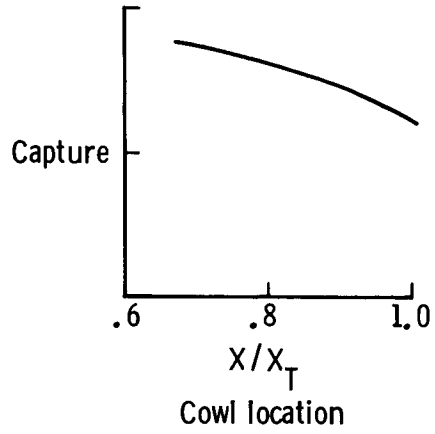

Fig. 15.- Inlet capture as a function of cowl location for strut compression angle, θ_s = 9°.

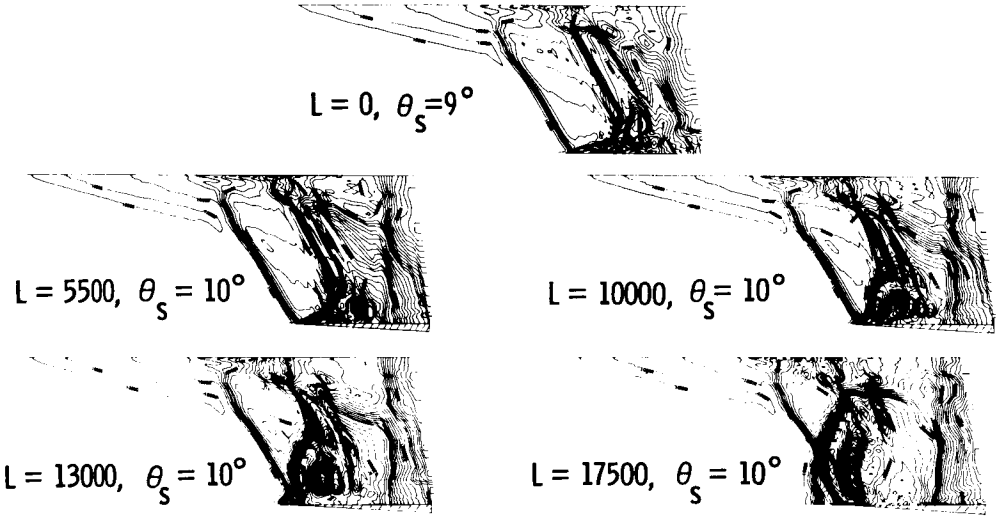

Fig. 16.- Pressure contours in the symmetry plane of the inlet.

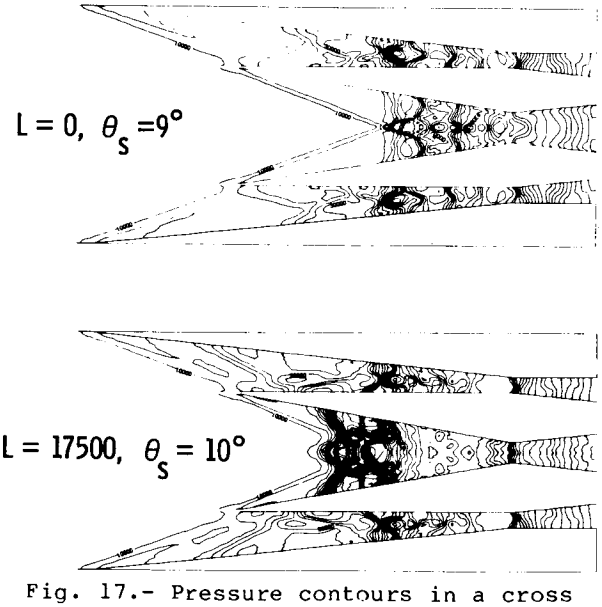

ORIGINAL PAGE IS
OF POOR QUALITY

Fig. 17.- Pressure contours in a cross plane located at 12% of the inlet height from the cowl plane.

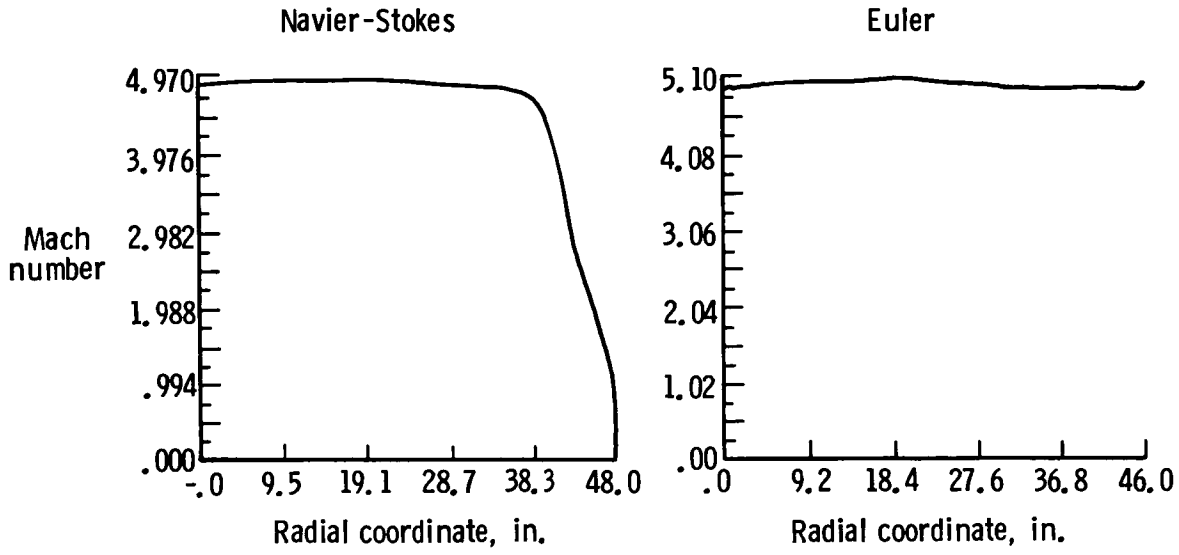

Fig. 18.- Exit plane Mach number profile in the designed Mach 5 nozzle.

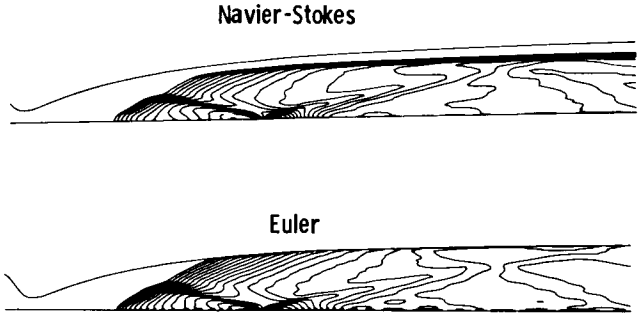

Fig. 19.- Mach number contours in the designed Mach 5 nozzle.